# 4D Neural Voxel Splatting: Dynamic Scene Rendering with Voxelized Guassian Splatting

Chun-Tin Wu<sup>1</sup>, Jun-Cheng Chen<sup>2</sup>
<sup>1</sup>National Taiwan University, <sup>2</sup>Academia Sinica



Figure 1. Our approach demonstrates remarkable memory efficiency and training speed, while achieving superior image quality

## **Abstract**

Although 3D Gaussian Splatting (3D-GS) achieves efficient rendering for novel view synthesis, extending it to dynamic scenes still results in substantial memory overhead from replicating Gaussians across frames. To address this challenge, we propose 4D Neural Voxel Splatting (4D-NVS), which combines voxel-based representations with neural Gaussian splatting for efficient dynamic scene modeling. Instead of generating separate Gaussian sets per timestamp, our method employs a compact set of neural voxels with learned deformation fields to model temporal dynamics. The design greatly reduces memory consumption and accelerates training while preserving high image quality. We further introduce a novel view refinement stage that selectively improves challenging viewpoints through targeted optimization, maintaining global efficiency while enhancing rendering quality for difficult viewing angles. Experiments demonstrate that our method outperforms state-ofthe-art approaches with significant memory reduction and faster training, enabling real-time rendering with superior visual fidelity.

## 1. Introduction

Dynamic 3D scene reconstruction and novel view synthesis are recent research hotspots in computer vision with a widespread applications in virtual reality (VR), augmented reality (AR), and digital entertainment. Capturing and ren-

dering temporal phenomena—such as human motion or deformable objects—is essential for immersive experiences.

While Neural Radiance Fields (NeRF) [12] achieve photorealistic view synthesis in static scenes, extending them to dynamics faces key bottlenecks: long training times, slow inference, and poor scalability with temporal complexity. Acceleration methods like DirectVoxGO [20] and Instant-NGP [13] improve efficiency but remain limited by volumetric rendering. 3D Gaussian Splatting (3D-GS) [4] shifts toward explicit point-based rendering, enabling realtime performance, yet naive extensions to dynamics suffer from memory growth proportional to sequence length. Canonical-space methods like 4D-GS [24] reduce this but rely on heavy deformation networks and costly backward mapping. Recent advances attempt to balance efficiency and expressiveness: Ex4DGS [5] improves temporal consistency via explicit motion modeling, FreeTimeGS [23] decouples space and time for flexible representation, and LongVolCap [25] compresses long sequences effectively.

However, the practical deployment of these methods remains constrained by memory and training overhead, especially in the scenarios of embodied AI which has a critical demand for the resource consumption. For instance, Mobile robots on edge devices (e.g., NVIDIA Jetson with 4–8GB memory) must rapidly reconstruct and track dynamic scenes for navigation and interaction. Field robots likewise require scene adaptation within minutes, not hours, to operate effectively. Current methods often exceed available resources on edge or mid-range GPUs, forcing compromises

in scene complexity or hardware cost. The core challenge is thus: how to capture rich temporal dynamics while maintaining memory and computational efficiency for real-time, resource-constrained applications.

To address these limitations, we introduce 4D Neural Voxel Splatting (4D-NVS), which combines voxel-based efficiency with Gaussian splatting quality through learned temporal deformation. Our key insight is decoupling spatial structure from temporal dynamics: we generate neural Gaussians on-demand from persistent voxel anchors and apply unified deformations. This achieves  $\mathcal{O}(fV+F)$  memory complexity compared to traditional  $\mathcal{O}(N\cdot T)$  scaling, where V is the number of voxels, f is the feature dimension per voxel, F represents the deformation network parameters, N is the number of Gaussians, and T is the number of timestamps.s While our method builds upon established techniques (voxel-based generation from Scaffold-GS [10] and HexPlane decomposition [2]), we introduce several key innovations that distinguish our approach:

- Unified 4D Voxel Architecture: We extend 3D voxel grids to 4D by treating time as an additional dimension in the voxel feature space, enabling temporal-aware Gaussian generation that adapts both spatially and temporally. Unlike Scaffold-GS which generates static Gaussians, our voxels produce time-varying Gaussians through learned temporal features.
- Selective Deformation Strategy: Through extensive experimentation, we identified that deforming all Gaussian properties leads to training instability. We introduce a selective approach that only deforms geometric properties (position, scale, rotation) while keeping appearance properties (color, opacity) fixed, significantly improving convergence and quality.
- View-Adaptive Refinement: We propose a novel refinement mechanism that identifies and selectively improves underperforming viewpoints through adaptive densification, addressing temporal inconsistencies without global overhead.
- Memory-Efficient Design: Our framework achieves  $\mathcal{O}(fV+F)$  memory complexity instead of  $\mathcal{O}(N\cdot T)$ . This makes dynamic scene rendering feasible on consumer GPUs.

To sum up, our 4D Neural Voxel Splatting successfully bridges computational efficiency and visual quality, enabling new possibilities for real-time dynamic visualization and interactive scene manipulation.

# 2. Related Works

In this section, we briefly review the relevant works of NeRF and Rasterization based methods for scene rendering.

## 2.1. NeRF-based Methods

Neural Radiance Fields (NeRF) [12] revolutionized novel view synthesis by representing scenes with MLPs that output view-dependent color and density. While achieving impressive visual fidelity, early NeRF models suffered from slow rendering due to costly volumetric ray marching. To address this, researchers introduced explicit representations like Plenoxels [16], which replaced MLPs with sparse voxel grids, and Instant-NGP [13], which employed multiresolution hashed grids for faster training and inference.

For dynamic scenes, methods like D-NeRF input time directly into the MLP, while more sophisticated approaches such as Nerfies [14] and NSFF [7] use explicit deformation networks to map points from canonical space to each frame. K-Planes [17] factorizes radiance fields into low-rank grids across space and time dimensions. Despite these advances, NeRF-based dynamic methods often face optimization challenges and increased memory requirements, struggling to capture complex non-rigid motions efficiently.

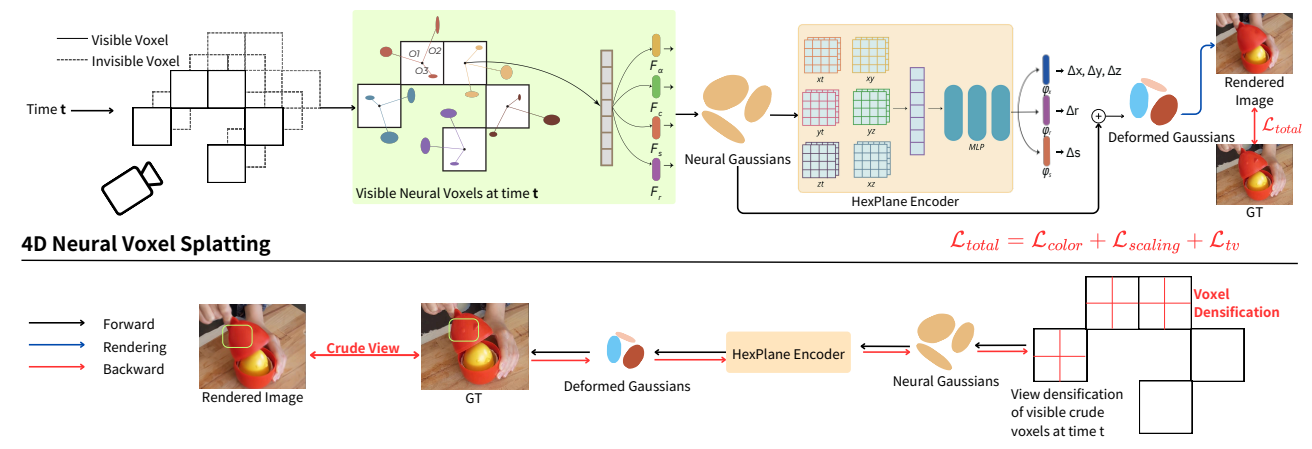
## 2.2. Rasterization Methods

3D Gaussian Splatting (3D-GS) [4] emerged as an efficient alternative, representing scenes with colored 3D Gaussian primitives rendered via projective splatting rather than volumetric rendering. This approach achieves real-time performance while maintaining high visual quality. Grid-based extensions like Scaffold-GS [10] generate neural Gaussians from anchor points, while SVRaster [21] uses sparse voxel-based rendering.

For dynamic scenes, 4D Gaussian Splatting (4D-GS) [24] extends 3D-GS with learned deformation fields to transform canonical Gaussians over time, avoiding the memory overhead of per-frame Gaussian sets. Other approaches include GaGS [11], which uses geometry-aware architectures for deformation modeling, and DynMF [8], which factorizes motion into trajectory bases. However, these methods either suffer from prolonged optimization times or demand excessive memory.

Recent advances include Ex4DGS [5] with explicit motion modeling, but requires complex trajectory computation increasing training overhead. FreeTimeGS [23] introduces temporal flexibility but struggles with memory scaling for long sequences. Long Volcap [25] addresses duration through compression yet sacrifices real-time performance due to decompression costs. While these methods target specific challenges, they introduce new computational bottlenecks that limit practical deployment.

In contrast to prior approaches, our method balances training efficiency and memory usage by integrating compact 4D neural voxel representations with selective property deformation, enabling accelerated convergence and real-time dynamic scene rendering with lower memory footprint.



#### **View Refinement**

Figure 2. Pipeline overview: (1) Initialize with voxel-based Gaussian splatting, (2) Generate neural Gaussians with temporal information, (3) Apply HexPlane temporal corrections, (4) Optimize with color loss, total variation loss, and scaling regularization, (5) View refinement stage for underperforming viewpoints through adaptive densification.

# 3. Preliminaries

# 3.1. 3D Gaussian Splatting

3D Gaussian Splatting (3D-GS) [4] represents scenes using anisotropic 3D Gaussians, each defined by a mean position  $\mu \in \mathbb{R}^3$  and covariance matrix  $\Sigma$ :

$$G(x) = e^{-\frac{1}{2}(x-\mu)^{\top} \Sigma^{-1}(x-\mu)},$$
 (1)

where the covariance matrix is constructed as  $\Sigma = RSS^TR^T$  using scaling matrix S and rotation matrix R. Each Gaussian has associated color c and opacity  $\alpha$  (modeled with spherical harmonics) .

Unlike volumetric rendering, 3D-GS projects Gaussians onto the image plane as 2D Gaussians and applies  $\alpha$ -blending:

$$C(x') = \sum_{i=1}^{N} c_i \alpha_i \prod_{j=1}^{i-1} (1 - \alpha_j),$$
 (2)

where x' is the pixel position,  $\alpha$  depends on the pixel position x' and N is the number of overlapping Gaussians. This tile-based rasterization enables real-time rendering with differentiable optimization.

## 3.2. Scaffold-GS: Grid-Based Gaussian Generation

Scaffold-GS [10] generates Gaussians from structured anchor points rather than optimizing individual primitives. Starting from a sparse point cloud  $P \in \mathbb{R}^{M \times 3}$ , it creates voxel centers:

$$\mathbf{V} = \left\{ \left| \frac{\mathbf{P}}{\epsilon} \right| \right\} \cdot \epsilon, \tag{3}$$

where  $\epsilon$  is the voxel size. Each voxel center  $v \in V$  serves as an anchor with local features  $f_v$ , scaling factor  $l_v \in \mathbb{R}^3$ , and k learnable offsets  $O_v \in \mathbb{R}^{k \times 3}$ .

Neural Gaussians are generated on-demand within the viewing frustum. For each visible anchor, k Gaussians are spawned with positions  $\mu_i = x_v + O_i \cdot l_v$ , while attributes (opacity, color, scale, rotation) are decoded from anchor features using MLPs conditioned on viewing direction and distance. This approach significantly reduces memory requirements compared to storing explicit Gaussians for the entire scene.

# 4. Method

#### 4.1. Overview

Our 4D Neural Voxel Splatting (4D-NVS) framework addresses the challenge of efficiently rendering dynamic scenes by extending traditional 3D voxel representations into the temporal domain. The core insight is that while 3D voxels effectively capture spatial structure, dynamic scenes require an additional temporal dimension. We achieve this through a three-stage training approach:

- Coarse Initialization. We initialize the spatial voxel structure using mixed timestamps to establish a foundational geometric representation. This stage focuses on learning the basic scene structure without temporal deformation.
- 2. **Fine Temporal Training.** We activate the HexPlane deformation module and train the full temporal model. During this stage, we also identify poorly reconstructed viewpoints for subsequent refinement.
- 3. **View Refinement.** We focus training exclusively on the identified crude viewpoints using more aggressive densification parameters, improving quality in challenging regions without affecting well-performing areas.

The key insight behind our method is the decoupling of

spatial representation from temporal dynamics. Rather than storing explicit primitives for each frame, we generate neural Gaussians on-demand from a persistent voxel grid and apply learned temporal deformations.

## 4.2. Initialization and Voxel Setup

We initialize neural voxels using the sparse point cloud from Structure-from-Motion (SfM) [18], distributing voxel centers to ensure comprehensive spatial coverage. The scene is first trained using Scaffold-GS [10] for 3K iterations with mixed timestamp samples to establish a foundational geometric representation.

## 4.3. Neural Gaussian Generation

**On-Demand Generation.** Unlike existing methods that pre-compute and store Gaussians, our approach generates neural Gaussians dynamically based on viewing conditions and temporal context. This represents a fundamental shift from static storage to dynamic computation, enabling both memory efficiency and view-dependent optimization.

At each timestamp t, we perform visibility culling to identify voxels within the camera frustum, significantly reducing computational overhead from  $\mathcal{O}(N)$  to  $\mathcal{O}(V_{visible})$  where  $V_{visible} \ll N$ . For each visible voxel v, we generate k neural Gaussians with positions:

$$\mu_i = x_v + O_i \cdot l_v, \quad i = 0, \dots, k - 1,$$
 (4)

where  $x_v \in \mathbb{R}^3$  is the voxel center position,  $O_i \in \mathbb{R}^3$  are learnable offset vectors for each of the k Gaussians, and  $l_v \in \mathbb{R}^3$  is the voxel's spatial extent (scale factor).

Gaussian attributes are decoded using dedicated MLPs that take anchor features  $f_v$ , viewing distance  $\delta_{vc}$ , and directional vector  $\vec{d}_{vc}$  as input:

$$\{\alpha_0, \dots, \alpha_{k-1}\} = F_{\alpha}(f_v, \delta_{vc}, \vec{d}_{vc}), \tag{5}$$

$$\{c_0, \dots, c_{k-1}\} = F_c(f_v, \delta_{vc}, \vec{d}_{vc}),$$
 (6)

$$\{s_0, \dots, s_{k-1}\} = F_s(f_v, \delta_{vc}, \vec{d}_{vc}),$$
 (7)

$$\{r_0, \dots, r_{k-1}\} = F_r(f_v, \delta_{vc}, \vec{d}_{vc}),$$
 (8)

where  $F_{\alpha}$ ,  $F_{c}$ ,  $F_{s}$ , and  $F_{r}$  are MLPs for opacity, color, scale, and rotation respectively.

## 4.4. Dynamic Gaussians Deformation

**Unified 4D Representation.** Our method introduces a novel temporal modeling approach that treats space and time as a unified 4D manifold while maintaining computational efficiency. Unlike previous methods that either use separate deformation networks for each Gaussian or employ expensive per-frame optimization, we leverage a shared HexPlane decomposition that captures temporal correlations across the entire scene.

To capture dynamic motion, we employ HexPlane [17] decomposition, encoding 4D space into six planes with multi-resolution temporal features  $f_h$ . Specifically, HexPlane factorizes the 4D space-time volume into six 2D planes: three spatial planes (XY, XZ, YZ) and three spacetime planes (XT, YT, ZT). For a 4D point (x, y, z, t), we extract features via bilinear interpolation from each plane and aggregate them:

$$f_h = \sum_{p \in \{XY, XZ, YZ, XT, YT, ZT\}} Interp_p(x, y, z, t).$$
 (9)

This decomposition provides several advantages over direct 4D parameterization: (1) significantly reduced memory footprint (2) natural handling of temporal correlations, and (3) efficient gradient flow during optimization. A compact MLP  $\phi_d$  integrates these features:

$$f_d = \phi_d(f_h), \tag{10}$$

where  $\phi_d$  is a shallow network for computational efficiency. Separate deformation decoders predict position, rotation, and scale changes:

$$\Delta \mu = \varphi_x(f_d),\tag{11}$$

$$\Delta r = \varphi_r(f_d),\tag{12}$$

$$\Delta s = \varphi_s(f_d),\tag{13}$$

where  $\varphi_x$ ,  $\varphi_r$ , and  $\varphi_s$  are single-layer MLPs that output 3D position offsets, quaternion rotations, and 3D scale factors, respectively.

The final deformed Gaussian values are  $(\mu',r',s')=(\mu+\Delta\mu,r+\Delta r,s+\Delta s)$ , while color and opacity remain unchanged to prevent error propagation, a design choice that emerged from our analysis of training stability in dynamic scenarios.

Selective Deformation Strategy. Through extensive experimentation, we discovered that deforming all five Gaussian properties (position, opacity, color, scale, rotation) leads to training instability and error accumulation. Specifically, we found that appearance properties (color and opacity) are highly sensitive to deformation errors, causing cascading failures during backpropagation. By keeping these properties fixed and only deforming geometric attributes, we maintain stable gradients while still capturing complex motion patterns.

# 4.5. Optimization

Our loss function combines multiple terms for robust optimization:

$$\mathcal{L} = \mathcal{L}_{color} + \lambda_{tv} \mathcal{L}_{tv} + \lambda_{vol} \mathcal{L}_{vol}, \tag{14}$$

where  $\mathcal{L}_{color} = \mathcal{L}_1 + \lambda_{SSIM} \mathcal{L}_{SSIM}$  ensures pixel accuracy and structural coherence,  $\mathcal{L}_{tv}$  enforces spatial smoothness

in the HexPlane, and  $\mathcal{L}_{vol} = \sum_{i=1}^{N_{ng}} \mathbf{s}_{\mathbf{x}i} \cdot \mathbf{s}_{\mathbf{y}_i} \cdot \mathbf{s}_{\mathbf{z}i}$  prevents oversized Gaussians.

For density control, we grow anchors in high-gradient regions and prune those producing consistently low-opacity Gaussians.

## 4.6. View Refinement

**Motivation.** During training, we observed that certain viewpoints consistently under-perform due to large deformations, complex occlusions, or rapid temporal changes. Rather than applying uniform densification across all views—which wastes computational resources on already well-reconstructed areas—we developed an adaptive refinement strategy that identifies and specifically improves problematic viewpoints while maintaining global efficiency.

**Crude View Selection.** We implement two complementary strategies for identifying crude viewpoints that require refinement:

**1. PSNR-based Detection.** We track the PSNR of each rendered view and compare it against an exponentially weighted moving average (EMA) to identify statistical outliers:

$$PSNR_i < (1 + \gamma) \cdot EMA_{PSNR}, \tag{15}$$

where  $\gamma$  starts at 0.05 and gradually decays to 0.02 during training to become more selective as optimization progresses. The EMA is updated with momentum 0.4 to balance responsiveness and stability:

$$EMA_{PSNR} = 0.4 \cdot PSNR_{current} + 0.6 \cdot EMA_{PSNR}.$$
 (16)

**2. Gradient-based Detection.** For scenarios where gradient information reveals optimization difficulties not captured by quality metrics, we track the gradient magnitude of viewspace points and identify views with abnormally high gradients indicating convergence issues:

$$\|\nabla \mathcal{L}_{\text{view}}\| > (1 + \gamma) \cdot \text{EMA}_{\text{grad}}.$$
 (17)

This dual-criteria approach ensures robust detection across different failure modes—quality-based detection captures rendering artifacts while gradient-based detection identifies optimization instabilities.

Identified viewpoints are added to a refinement stack with associated metadata including failure type (quality vs. gradient), severity score, and temporal consistency flags. Views appearing consecutively in multiple frames receive higher priority for refinement.

**Adaptive Quality Enhancement.** For views identified as crude, we apply specialized training in a dedicated third stage (14k iterations) that focuses computational resources exclusively on problematic areas:

**1. Focused Training.** Only crude viewpoints from the adaptive camera list are used for training, with sampling probability weighted by severity scores. This concentrates

gradient updates on areas that need improvement most, avoiding dilution of learning signals from well-performing regions.

- **2. Adjusted Thresholds.** We use more aggressive densification parameters specifically tuned for challenging views: These lower thresholds encourage more frequent Gaussian splitting and pruning in problematic regions.
- **3. Enhanced Gaussian Generation.** The reduced thresholds facilitate creation of additional Gaussians in regions with complex motion patterns, fine-grained occlusions, or temporal discontinuities. New Gaussians inherit temporal features from nearby anchors and undergo immediate deformation field training to capture local dynamics.

This targeted approach enhances overall quality and temporal consistency without computational overhead on well-performing areas, achieving 0.5-1.2 dB PSNR improvements on challenging viewpoints while maintaining global rendering efficiency.

# 5. Experiments

# **5.1. Setup**

**Setup.** We set k=10 Gaussians per Neural Voxel and feature dimension  $f_v \in \mathbb{R}^{32}$ . HexPlane grids use resolution [64, 64, 64, 150] for DyNeRF and [64, 64, 64, 25] for HyperNeRF with scale multipliers [1, 2]. Training consists of 3k initialization iterations, 14k main training, and 14k view refinement iterations.

**Implementation Details.** We use Adam optimizer with learning rates: Gaussian offsets (0.01), color MLP (0.008), opacity MLP (0.002), rotation/scaling MLPs (0.004), Hex-Plane grids (0.0016), deformation MLPs (0.00016). All rates decay to 1/10 initial values by iteration 14,000.

Loss weights:  $\lambda_{vol}=0.015$  for volume regularization and  $\lambda_{tv}=0.0002$  for total variation loss. Densification threshold:  $\tau_g=0.0002$  (coarse)  $\rightarrow 0.0001$  (refinement); opacity threshold:  $\tau_{\alpha}=0.05 \rightarrow 0.03$ .

**Dataset.** HyperNeRF [15]: 1-2 cameras with straightforward motion. Neu3D [6]: 15-20 static cameras with complex motion. COLMAP initialization from first frame (Neu3D) or 200 random frames (HyperNeRF), yielding 5,000-20,000 initial points for voxel grid initialization.

## 5.2. Results

Quantitative Results. To assess the quality of novel view synthesis, we conducted benchmarking against several state-of-the-art methods in the field. The results are summarized in Table 1 and Table 2. On HyperNeRF, our method achieves 28.5 PSNR while using the least memory (3,050 MiB) and fastest training time (13 minutes). On Neu3D, we maintain competitive quality (33.12 PSNR) with real-time rendering at 43 FPS—an order of magnitude faster than Im4D (5 FPS) and MSTH (2 FPS). This combination

Model	PSNR(dB)↑	MS-SSIM↑	Times↓	FPS↑	Memory Usage(MiB)↓
Nerfies [14]	22.2	0.803	$\sim$ hours	< 1	-
3D-GS* [4]	19.7	0.68	40 mins	55	-
Scaffold-GS* [10]	20.7	0.688	35 mins	55	-
HyperNeRF [15]	22.4	0.814	32 hours	< 1	-
TiNeuVox-B [3]	24.3	0.836	18 mins**	1	21,558**
4D-GS [24]	25.2	0.845	25 mins**	34	4,500**
GAGS [11]	24.26	0.83	120 mins**	11	6875**
Ours w/o. Refining	25.8	0.846	10 mins†	45	3,050
Ours	28.5	0.872	13 mins†	44	3,050

<sup>\*: 3</sup>D-GS, Scaffold-GS are trained on randomly sampled timestamps from all frames, without temporal modeling.

\*\*: The training time and memory is re-evaluated by us on a single RTX 4090 GPU.

Table 1. Quantitative results on the HyperNeRF [15] VRIG dataset, rendered at a resolution of  $960 \times 540$ . The best and second best results are highlighted in red and yellow, respectively. Our method performed the best compared to other methods, while using the least memory and training time.

Model	PSNR(dB) ↑	D-SSIMJ.	Time	FPS↑
	. , , ,	•	- •	
NeRFPlayer [19]	30.69	0.034	6 hours	0.045
HyperReel [1]	31.10	0.036	9 hours	2.0
HexPlane [2]	31.70	0.014	12 hours	0.2
KPlanes [17]	31.63	-	1.8 hours	0.3
Im4D [9]	32.58	-	28 mins	5
MSTH [22]	32.37	0.015	20 mins	2
4D-GS(CVPR'24) [24]	31.15	0.016	32 mins	34
4D-GS(ICLR'24) [26]	31.91	0.015	105 mins	114
Ex4DGS[5]*	32.11	0.015	36 mins	25
Ours**	33.12	0.021	25 mins	43

<sup>\*:</sup> The training time and FPS is evaluated by us on a single RTX-4090.

Table 2. Quantitative results on the Neu3D [6] dataset. Note: rendering resolution is set to  $1352 \times 1014$ .

of high quality, minimal memory footprint, and real-time performance makes our approach ideal for practical deployment.

Qualitative Results. The qualitative results of our study, compared with several other methods, are shown in Figure 3, 4. These results demonstrate the effectiveness of our approach. With reduced training time, rendering time, and memory consumption, our method still produces competitive qualitative results compared to previous methods. In some cases, especially those with smaller movements, we manage to produce more detailed images.

## 5.3. Ablation Study

**Loss Design.** We present the ablation studies in Table 3 to highlight the differences in quantitative results regarding Volume regularization and Total Variation Loss. We also rendered images specifically focused on Volume regularization, as it had a significant impact on the qualitative results. As shown in Figure 6 without the volume regularization term  $\mathcal{L}_{vol}$ , we observe large Gaussians floating in front of the camera, causing the blurry effect on the image.

Loss		Metrics		
$\overline{\mathcal{L}_{vol}}$	$\mathcal{L}_{tv}$	PSNR	MS-SSIM	
-	-	22.73	0.67	
$\checkmark$	-	25.58	0.76	
-	$\checkmark$	24.89	0.78	
$\checkmark$	$\checkmark$	29.51	0.92	

Table 3. Comparison of PSNR, SSIM for ablation studies with Volume regularization and Total Variation Loss on HyperNeRF-Chicken without gradient-based detection.

	Metrics		
	PSNR	MS-SSIM	
Ours w/o. HexPlane	22.31	0.71	
Ours w/o. Refinement	28.61	0.88	
Ours w/o. View dependent sorting	29.31	0.91	
Ours w/o. Gradient-Based Detection	29.51	0.92	
Ours	31.28	0.94	

Table 4. Comparison of PSNR and SSIM for ablations on HyperNeRF-Chicken.

**Selective Deformation Strategy.** A key design choice in our method is the selective deformation of Gaussian properties. Table 5 demonstrates the impact of this strategy. When deforming all properties (including color and opacity), training becomes unstable and quality degrades. Our selective approach, which only deforms geometric properties (position, scale, rotation), maintains stable training while achieving better results.

**View Refinement.** We observed that some viewpoints were not reconstructed accurately, which we attribute to inconsistencies in the Gaussians. As shown in Table 4, the view refinement effectively enhances image quality by refining consistency across viewpoints, as illustrated in Figure 7, re-

<sup>†:</sup> Training time includes 3k initialization iterations (approximately 2 minutes).

<sup>\*\*:</sup> We introduced gradient-selection selection in view refinement stage which improves the metrics

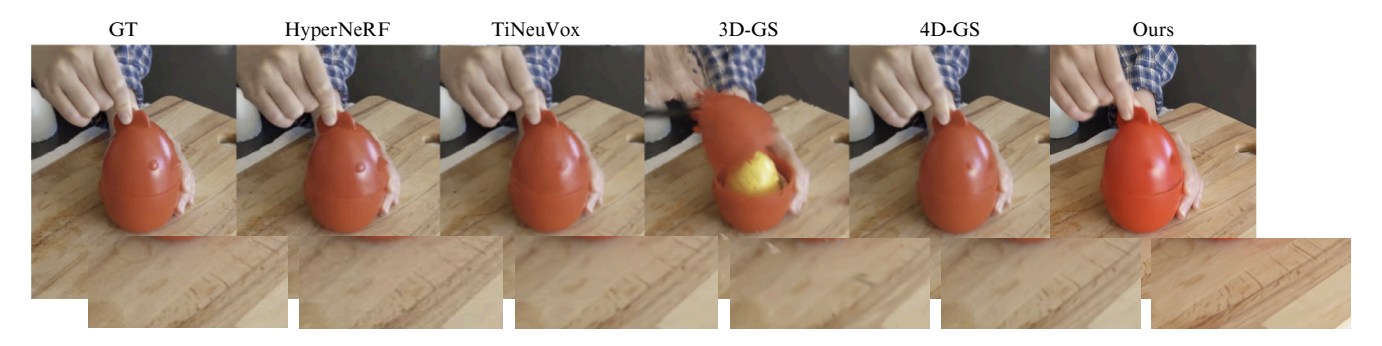


Figure 3. Visual comparisons of the proposed method on the HyperNeRF dataset with other methods. The proposed method achieves better rendering results.

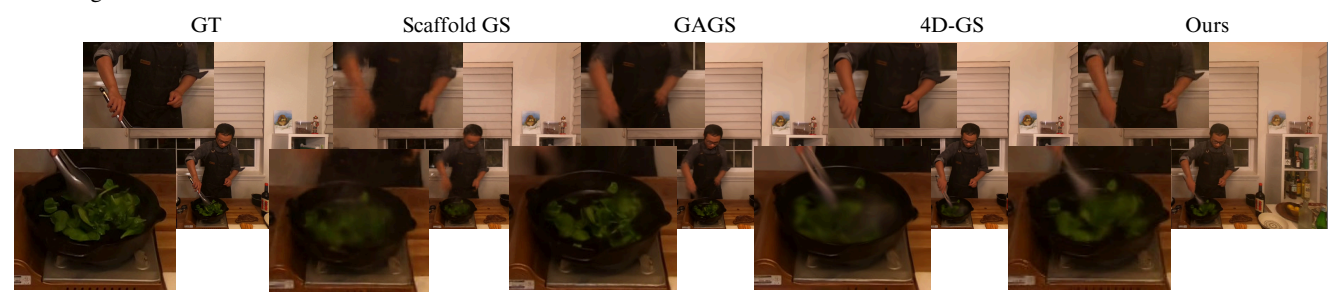


Figure 4. Visualization of the Neu3D dataset compared with other methods. From the visual illustration shown in the top and bottom left, the proposed method strikes a balance while the others either perform worse on the hand or the spinach in the pan. More rendering videos can be found in the supplementary materials.



Figure 5. Continuous Frames on HyperNeRF Dataset compared with 4DGS. *Top: Ours, Bottom: 4DGS*. The proposed method deliver a better rendering results with more details than 4DGS, which can be seen in the top right.

Deformation Strategy	PSNR	MS-SSIM	Training Stability
All Properties	26.42	0.81	Unstable
Geometric Only (Ours)	29.51	0.92	Stable
Appearance Only	24.18	0.73	Stable
No Deformation	22.31	0.71	Stable

Table 5. Ablation study on selective deformation strategy. Deforming only geometric properties achieves the best balance between quality and training stability.



Figure 6. Left: with  $L_{vol}$  Right: w/o.  $L_{vol}$ .

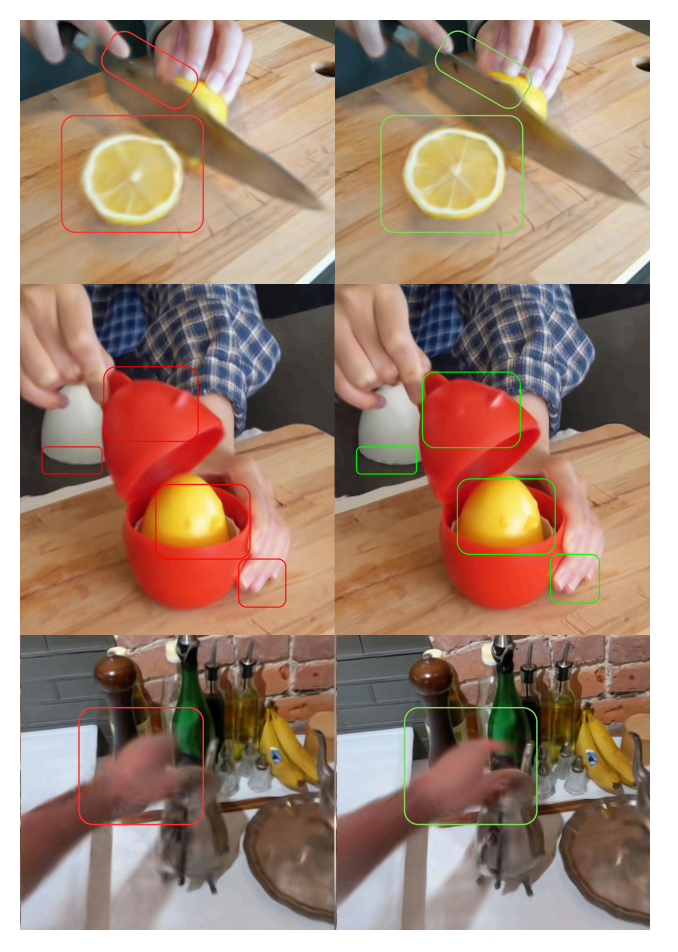


Figure 7. Left: w/o. view refinement. Right:with view refinement.

sulting in more visually appealing outcomes.

# 5.4. Memory and Speed Analysis

**Memory Usage.** Our method requires only 3,050 MiB, achieving 86% reduction vs. TiNeuVox-B (21,558 MiB), 32% vs. 4D-GS (4,500 MiB), and 56% vs. GaGS (6,875 MiB). This enables deployment on consumer hardware with limited GPU resources.

**Training Time.** Our model completes training in 17 minutes with refinement (13 minutes without), achieving 94% speedup vs. HyperNeRF (32 hours), 32% vs. 4D-GS (25 minutes), and 89% vs. GaGS (120 minutes). This enables rapid deployment in real-time interactive environments.

# 5.5. Limitations

Though our 4D Neural Voxel Splatting achieves rapid convergence and yields real-time rendering in many scenarios, a few key challenges remain.

**Large Motions.** The absence of initial points and inaccuracies in camera poses make it challenging to optimize the Gaussians effectively. Although incorporating view refinement has improved this issue, further enhancements in motion estimation are necessary for a complete solution.

**Popping Artifacts.** Although introducing view-dependent sorting solves the "static" part of the popping artifact, it is not entirely eliminated. Further enhancements in voxel representation and 3D Gaussians' rasterizing process are needed to completely remove the artifacts.

## 6. Conclusion

We introduced 4D Neural Voxel Splatting (4D-NVS), a method for real-time dynamic scene rendering that extends voxel representations to the temporal domain. By decoupling spatial structure from temporal dynamics through neural Gaussians and deformation fields, our approach achieves superior rendering quality with memory reduction and computational efficiency. 4D-NVS opens new avenues for real-time dynamic visualization and interactive scene manipulation across various applications.

## References

- [1] Benjamin Attal, Jia-Bin Huang, Christian Richardt, Michael Zollhöfer, Johannes Kopf, Matthew O'Toole, and Changil Kim. Hyperreel: High-fidelity 6-dof video with ray-conditioned sampling. arXiv preprint arXiv:2301.02238, 2023. 6
- [2] Ang Cao and Justin Johnson. Hexplane: A fast representation for dynamic scenes. In *Proceedings of the IEEE/CVF Conference on Computer Vision and Pattern Recognition (CVPR)*, pages 130–141, 2023. 2, 6
- [3] Jiemin Fang, Taoran Yi, Xinggang Wang, Lingxi Xie, Xiaopeng Zhang, Wenyu Liu, Matthias Nießner, and Qi Tian. Fast dynamic radiance fields with time-aware neural voxels. In SIGGRAPH Asia 2022 Conference Papers, 2022. 6

- [4] Bernhard Kerbl, Georgios Kopanas, Thomas Leimkuhler, and George Drettakis. 3d gaussian splatting for real-time radiance field rendering. *ACM Transactions on Graphics* (*ToG*), 42(4):1–14, 2023. 1, 2, 3, 6
- [5] Junoh Lee, ChangYeon Won, Hyunjun Jung, Inhwan Bae, and Hae-Gon Jeon. Fully explicit dynamic guassian splatting. In *Proceedings of the Neural Information Processing* Systems, 2024. 1, 2, 6
- [6] Tianye Li, Mira Slavcheva, Michael Zollhoefer, Simon Green, Christoph Lassner, Changil Kim, Tanner Schmidt, Steven Lovegrove, Michael Goesele, Richard Newcombe, et al. Neural 3d video synthesis from multi-view video. In Proceedings of the IEEE/CVF Conference on Computer Vision and Pattern Recognition (CVPR), pages 5521–5531, 2022. 5, 6
- [7] Zhengqi Li, Simon Niklaus, Noah Snavely, and Oliver Wang. Neural scene flow fields for space-time view synthesis of dynamic scenes. In Proceedings of the IEEE/CVF Conference on Computer Vision and Pattern Recognition (CVPR), 2021.
- [8] Zhan Li, Zhang Chen, Zhong Li, and Yi Xu. Spacetime gaussian feature splatting for real-time dynamic view synthesis. *arXiv preprint arXiv:2312.16812*, 2023. 2
- [9] Haotong Lin, Sida Peng, Zhen Xu, Tao Xie, Xingyi He, Hujun Bao, and Xiaowei Zhou. High-fidelity and real-time novel view synthesis for dynamic scenes. In SIGGRAPH Asia Conference Proceedings, 2023. 6
- [10] Tao Lu, Mulin Yu, Linning Xu, Yuanbo Xiangli, Limin Wang, Dahua Lin, and Bo Dai. Scaffold-gs: Structured 3d gaussians for view-adaptive rendering. In *Proceedings of the IEEE/CVF Conference on Computer Vision and Pattern Recognition (CVPR)*, pages 20654–20664, 2024. 2, 3, 4, 6
- [11] Zhicheng Lu, Xiang Guo, Le Hui, Tianrui Chen, Ming Yang, Xiao Tang, Feng Zhu, and Yuchao Dai. 3d geometry-aware deformable gaussian splatting for dynamic view synthesis. In Proceedings of the IEEE/CVF Conference on Computer Vision and Pattern Recognition, 2024. 2, 6
- [12] Ben Mildenhall, Pratul P. Srinivasan, Matthew Tancik, Jonathan T. Barron, Ravi Ramamoorthi, and Ren Ng. Nerf: Representing scenes as neural radiance fields for view synthesis. In ECCV, 2020. 1, 2
- [13] Thomas Müller, Alex Evans, Christoph Schied, and Alexander Keller. Instant neural graphics primitives with a multiresolution hash encoding. ACM Trans. Graph., 41(4):102:1–102:15, 2022. 1, 2
- [14] Keunhong Park, Utkarsh Sinha, Jonathan T. Barron, Sofien Bouaziz, Dan B. Goldman, Steven M. Seitz, and Ricardo Martin-Brualla. Nerfies: Deformable neural radiance fields. In *Proceedings of the IEEE/CVF International Conference* on Computer Vision (ICCV), pages 5865–5874, 2021. 2, 6
- [15] Keunhong Park, Utkarsh Sinha, Peter Hedman, Jonathan T. Barron, Sofien Bouaziz, Dan B Goldman, Ricardo Martin-Brualla, and Steven M. Seitz. Hypernerf: A higher-dimensional representation for topologically varying neural radiance fields. ACM Trans. Graph., 40(6), 2021. 5, 6
- [16] Sara Fridovich-Keil and Alex Yu, Matthew Tancik, Qinhong Chen, Benjamin Recht, and Angjoo Kanazawa. Plenoxels: Radiance fields without neural networks. In CVPR, 2022. 2

- [17] Sara Fridovich-Keil and Giacomo Meanti, Frederik Rahbæk Warburg, Benjamin Recht, and Angjoo Kanazawa. K-planes: Explicit radiance fields in space, time, and appearance. In CVPR, 2023. 2, 4, 6
- [18] Johannes Lutz Schönberger and Jan-Michael Frahm. Structure-from-motion revisited. In *Proceedings of the IEEE Conference on Computer Vision and Pattern Recognition* (CVPR), pages 4104–4113, 2016. 4
- [19] Liangchen Song, Anpei Chen, Zhong Li, Zhang Chen, Lele Chen, Junsong Yuan, Yi Xu, and Andreas Geiger. Nerfplayer: A streamable dynamic scene representation with decomposed neural radiance fields. *IEEE Transactions on Visu*alization and Computer Graphics, 29(5):2732–2742, 2023.
- [20] Cheng Sun, Min Sun, and Hwann-Tzong Chen. Direct voxel grid optimization: Super-fast convergence for radiance fields reconstruction. *arXiv* preprint arXiv:2306.01496, 2023. 1
- [21] Cheng Sun, Jaesung Choe, Charles Loop, Wei-Chiu Ma, and Yu-Chiang Frank Wang. Sparse voxels rasterization: Real-time high-fidelity radiance field rendering. *ArXiv*, abs/2412.04459, 2024. 2
- [22] Feng Wang, Zilong Chen, Guokang Wang, Yafei Song, and Huaping Liu. Masked space-time hash encoding for efficient dynamic scene reconstruction. In Advances in Neural Information Processing Systems (NeurIPS), 2023. 6
- [23] Yifan Wang, Peishan Yang, Zhen Xu, Jiaming Sun, Zhanhua Zhang, Yong Chen, Hujun Bao, Sida Peng, and Xiaowei Zhou. Freetimegs: Free gaussian primitives at anytime anywhere for dynamic scene reconstruction. In CVPR, 2025. 1,
- [24] Guanjun Wu, Taoran Yi, Jiemin Fang, Lingxi Xie, Xiaopeng Zhang, Wei Wei, Wenyu Liu, Qi Tian, and Xinggang Wang. 4d gaussian splatting for real-time dynamic scene rendering. In Proceedings of the IEEE/CVF Conference on Computer Vision and Pattern Recognition (CVPR), pages 20310–20320, 2024. 1, 2, 6
- [25] Zhen Xu, Yinghao Xu, Zhiyuan Yu, Sida Peng, Jiaming Sun, Hujun Bao, and Xiaowei Zhou. Representing long volumetric video with temporal gaussian hierarchy. ACM Transactions on Graphics, 43(6), 2024. 1, 2
- [26] Zeyu Yang, Hongye Yang, Zijie Pan, and Li Zhang. Realtime photorealistic dynamic scene representation and rendering with 4d gaussian splatting. In *International Conference* on *Learning Representations (ICLR)*, 2024. 6

# 4D Neural Voxel Splatting: Dynamic Scene Rendering with Voxelized Guassian Splatting

# Supplementary Material

# 7. Supplementary Material

### 7.1. Introduction

In the supplementary material, we provide additional details and videos on our hyperparameter settings in 8. More qualitative results are presented in 9, further ablation study results are discussed in 9.1, and additional discussions are included in 10.

# 8. Hyperparameters

### 8.1. Gaussian Generation

The following learning rates are configured for the Gaussian generation process.

**Offset.** The learning rate for the offset vector starts at  $1\times 10^{-2}$  and decays to  $1\times 10^{-5}$ .

**Opacity.** The learning rate for MLP with opacity starts at  $2\times 10^{-3}$  and decreases to  $2\times 10^{-6}$ .

Covariance. This includes rotation and scaling. The learning rate for these MLPs starts at  $4\times10^{-3}$  and decays to  $4\times10^{-6}$ .

Color. The learning rate for color MLP starts at  $8\times 10^{-3}$  and decays to  $5\times 10^{-7}$ .

## 8.2. HexPlane Module

The following learning rates are configured for the Hex-Plane module:

**HexPlane Feature.** The learning rate for the HexPlane feature starts at  $1.6 \times 10^{-3}$  and decays to  $1.6 \times 10^{-4}$ .

**Deformation Decoder.** The learning rate for the decoder starts at  $1.6 \times 10^{-4}$  and decays to  $1.6 \times 10^{-5}$ .

## 8.3. Iterations

For initializing the Neural Voxels, we train for 3000 iterations on static scenes. Next, we train for 14,000 iterations with temporal information included and HexPlane activated. Finally, we perferformed another 14,000 iterations for view refinement on underperforming views.

## 8.4. Pruning and Growing

Anchor points are dynamically pruned and grown during training:

**Growing.** Growing starts at iteration 500 and is activated every 100 iterations until iteration 12,000.

**Pruning.** Pruning starts at iteration 500 and is activated every 100 iterations throughout the training.

## 9. Results

Since we are unable to render videos in the main paper, this section includes several videos comparing our method to 4D-GS as well as additional videos demonstrating our performance in photorealistic rendering.

**Appendix 1:** Comparison of our method with 4D-GS on the HyperNeRF-Interp dataset.

**Appendix 2** Rendered scenes in HyperNeRF showcasing our qualitative results.

**Appendix 3** We achieved PSNR of 22.15 Rendered a scene in a monocular dataset Ub4D without any geometry priors to showcase our ability to reconstruct a monocular scene.

### 9.1. Ablation Studies

This section demonstrates the effectiveness of our method by rendering with and without view refinement. The results are provided in **Appendix 4.** 

#### 10. Discussions

## 10.1. Limitations of the Current Approach

Although our 4D Neural Voxel Splatting method achieves significant improvements in memory efficiency, training speed, and rendering quality, there are still limitations. For example, dynamic scenes with large motions or significant occlusions present challenges for Gaussian generation and deformation, requiring further enhancements in motion modeling and temporal consistency.

# 10.2. Potential Applications and Impacts

Our method holds promise for various applications, including virtual reality, augmented reality, robotics, and the creation of digital content. By enabling efficient and high-quality rendering of dynamic scenes, it can facilitate advancements in immersive environments, simulation training, and real-time visual effects.

## 10.3. Future Work Directions

There are several avenues for future research. One direction involves improving the robustness of Gaussian deformation fields to better handle large motions and noisy camera poses. Another promising area is optimizing the voxel representation to entirely eliminate the Gaussian "popping artifact". Furthermore, exploring hybrid approaches that combine explicit and implicit representations could enhance scalability without sacrificing efficiency.